Journal of Petroleum Exploration and Production Technology (2023) 13:1099–1106
https://doi.org/10.1007/s13202-022-01594-y

ORIGINAL PAPER - PRODUCTION ENGINEERING

Study on deposit formation model in sulfide-containing natural gas environment

Liu Yongliang[1] · Ou Zhidong[1] · Deng Hongda[2] · Zhang Zewei[1] · Zeng Yunfan[1] · Liu Jian[1]

Received: 9 November 2021 / Accepted: 10 December 2022 / Published online: 19 December 2022

Abstract
The breathing pipe of a produced water storage tank in a sulfide-containing natural gas station is prone to deposit formation, which leads to pipeline blockage. In this study, scanning electron microscopy (SEM), energy-dispersive X-ray spectroscopy (EDS), and X-ray diffraction (XRD) analyses of the deposit in breathing pipe show that the deposit is composed of elemental sulfur and corrosion scales of ferrous polysulfide and ferrous sulfate. Existing deposit formation prediction models cannot predict the formation of elemental sulfur and corrosion scales in sulfide-containing environments. Herein, based on thermodynamic models of elemental sulfur and corrosion scale formation, deposit formation models of elemental sulfur, ferrous polysulfide, and ferrous sulfate scale formation are established. It is found that deposition of elemental sulfur and ferrous polysulfide increases with decreasing temperature of the breathing tube. Corrosion of pipe in the precipitating corrosive water leads to higher activity of $[Fe^{2+}]$ on the inner wall of the pipe carried by the sulfide-containing natural gas. Consequently, ferrous polysulfide and ferrous sulfate are easily deposited when the activity products of ferrous, sulfide, and sulfate ions are higher than the thermodynamic solubility product constant. The aforementioned prediction models are applied to predict the deposition of ferrous polysulfide, ferrous sulfate corrosion scale, and elemental sulfur using the chemical composition data of gas and precipitating water in the breathing pipe of the produced water tank of TB101-X1 well. The prediction results of the models are consistent with those of actual chemical composition analysis, which verifies the accuracy and reliability of the models.

Keywords Sulfide-containing natural gas · Breathing pipe · Sulfide · Ferrous polysulfide · Ferrous sulfate · Scale · Prediction model

Introduction

A serious problem in the production of high sulfide-containing natural gases is the presence of sulfur and scale deposits in production facilities. Herein, sulfur and scale deposits can cause a substantial and drastic reduction in the velocity of fluids. In the produced water treatment facilities, sulfide-containing gas-saturated produced water is stored in a water tank for environmental consideration, whereas the sulfide-containing natural gas carrying the produced water is distinctly separated from the produced water owing to the decrease in pressure and temperature in the produced water tank. Subsequently, this natural gas is poured into the breathing pipe and finally discharged to the vent for combustion treatment. With the decrease in the temperature and velocity of flow of sulfide-containing natural gas in the long breathing pipe, elemental sulfur and carried produced water precipitate from sulfide-containing natural gas. These precipitates adhere to the inner wall of the breathing pipe owing to the long-term direct contact between the breathing pipe and precipitating water saturated with hydrogen sulfide. Subsequently, deposits are formed through physical and chemical reactions.

Although the deposit components are specific to their gas fields, most deposits are generally composed of a limescale or corrosion scale. The limescale may include $CaSO_4$, $MgSO_4$, $BaSO_4$, $SrSO_4$, and a predominant amount of

✉ Liu Yongliang
26407443@qq.com; liuyongl@petrochina.com.cn

[1] PetroChina Southwest Oil and Gas Field Company, Northeast Sichuan Gas Field, (635000) Northeast Sichuan Gas Mine, No.436 Fenghuang Avenue, Xiwai, Dazhou 635000, China

[2] Chongqing University of Science and Technology, Chongqing 401331, China

$CaCO_3$ (Du 2016). There have been many studies on lime-scaling thermodynamics, lime-scaling probability prediction models, lime-scaling rates, and limescale prevention and removal measures (Shahzad et al. 2018; Kan et al. 2019). Environmental factors influence limescale formation. For example, the solubility of lime-scaling salts, such as $CaSO_4$, increases drastically with increasing temperature within lower temperature range and decreases within higher temperature range, so the solubility of $CaSO_4.2H_2O$ has the maximum value at the investigated temperatures. In contrast, the solubility of $BaSO_4$ and $SrSO_4$ decreases with increasing temperature. Furthermore, the scaling probability increases with decreasing pressure. Scale formation takes place readily with the increase in the pH of the solution. Additionally, the smaller the flow velocity, the stronger the scaling probability (Song et al. 2011). At present, the saturation index models (Oddo–Tomson saturation index model, Davis–Stiff saturation index model, Ryznar stability index model, and CaSO4 scaling index model) are used to calculate the relevant scaling index, determine the scaling type, and predict the scaling probability (Yu et al. 1999; Tang et al. 2011; Liu et al. 2016). Moreover, the saturation index model has been used to predict the formation of different types of limescales, such as carbonate scale, sulfate scale, scale consisting of carbonate and sulfate, and silica scale, in the production process of oil and gas fields. The limitations of various models have been pointed out (Shun et al. 1999; Kan et al. 2019). In addition to the formation of scales, the pipe will be corroded in a wet hydrogen sulfide environment. Iron ions generated during corrosion react with hydrogen sulfide, sulfate ions, and hydroxide ions in the environment to generate corrosion scales, such as sulfide, sulfate, oxide, and carbonate (Shahzad et al. 2018). Among above corrosion scales, iron sulfide behaves at least nine phases reported from field studies, such as mackinawite, troilite, pyrrhotite, and pyrite (Nasr-El-Din and Al-Humaidan 2001; Verri et al. 2017; Liu et al. 2017; Ramanathan et al. 2020). FeS solid can transform from one phase to another with the dependence of many factors, including temperature, solution pH, aging time, ionic strength, and oxidation potential (Rickard and Luther 2007; Lemire et al. 2013; Liu et al. 2017; Ahmed et al. 2020). Pyrite is typically the most thermodynamically stable phase, which have been built the thermodynamical prediction model (Bryndzia et al. 2020). It has also been predicted that mackinawite (FeS_m), with chemical stoichiometry of Fe to S 1:1, is usually kinetically favored and is the primary corrosion and precipitation product. A novel thermodynamic model for iron sulfide solubility prediction, which combines Pitzer theory and ion complexation, has been developed (Wang et al. 2022). And the stability constant of $FeSO_4$ complex has been calculated (Cifuentes et al. 2006). With the decreasing temperature, the limescales and corrosion scale are deposited on the inner surface of pipe. Corrosion under deposits may occur in oil and gas environments (Obot et al. 2021). When the pressure increases, the blocked and corroded pipe may burst owing to the limescale and corrosion scale and result in adverse consequences. The scaling probability is predicted primarily based on the saturation index model. However, there is no prediction study on the scaling probability of coexisting corrosion scales and elemental sulfur scales in sulfide-containing environments.

The content of hydrogen sulfide in the sulfide-containing natural gas stations and mineralization in the produced water is high, which leads to serious deposit formation. Based on the thermodynamics of deposit formation, the deposit prediction models proposed in this study as well as other prediction models are validated. Validation is performed by combining the data of chemical composition of the gas and the precipitating water in the breathing pipe, which is poured through the sulfide-containing natural gas with the carried water.

Scale identification of breathing pipe

The TB101-X1 well was produced on November 15, 2008. By December 31, 2020, the accumulated gas production was 6.76×10^8 m^3 and the cumulative water production was 1.73×10^4 m^3. The breathing pipe of the produced water tank was blocked and perforated thrice in November 2015, July 2017, and April 2020 (Fig. 1). Figure 1 shows different formation of deposits at the opposite ends of the breathing pipe. An obvious black, dense, and hard deposit was formed on the inner wall of the front-end of the breathing pipe, among which earthy red and yellow white deposits are distributed on the black scale in the 6 o' clock direction. The bottom of the tube was thicker than the top of the pipe. The rear portion of the breathing pipe was completely clogged by deposits. In addition, similar deposits and blockage degrees were found in the breathing pipe of well L14.

Samples of deposits inside the breathing pipe of the sulfide-containing natural gas station were taken and observed using an S-3700 N scanning electron microscope (SEM). It was found that the scale was dense, and the elements of the scale were composed of S, O, and Fe, among which S was the predominant element (Fig. 2).

The composition of the deposit in the breathing pipe of the TB101-X1 and L14 wells was analyzed by X-ray diffraction (XRD). The scale was composed of elemental sulfur S_8, ferrous polysulfide and ferrous sulfate (S_8 47.2wt. %, $FeSO_4(H_2O)_4$ 29.3wt.%, FeS_2 16.7wt.%, Fe_3S_4 6.8wt.%), wherein ferrous polysulfide consisted of sulfides with different atomic ratios. The deposit inside the L14 gas field water tank breathing riser was composed of S_8, ferrous polysulfide and $FeSO_4$ (S_8 53.8%, FeS 22.6%, $FeSO_4$ 43.6%) (Fig. 3). No ferrous carbonate was found in the deposits formed in the

Fig. 1 Morphologies of deposit at front end and rear end of breathing pipe

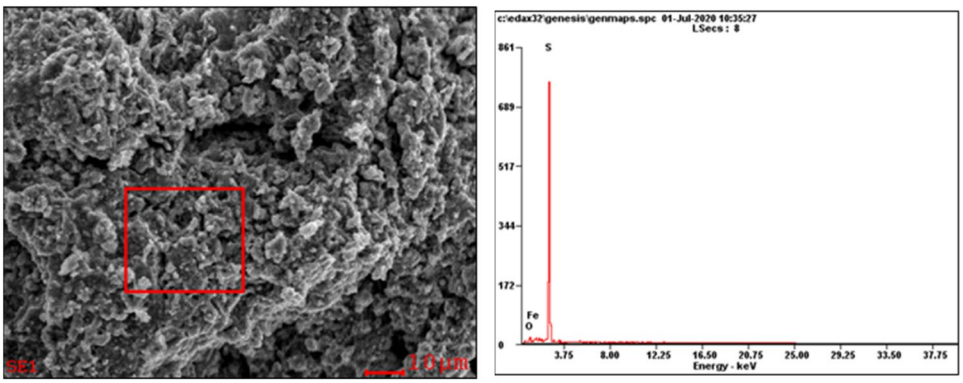

Fig. 2 Micro-morphology and element composition of deposit in breathing pipe

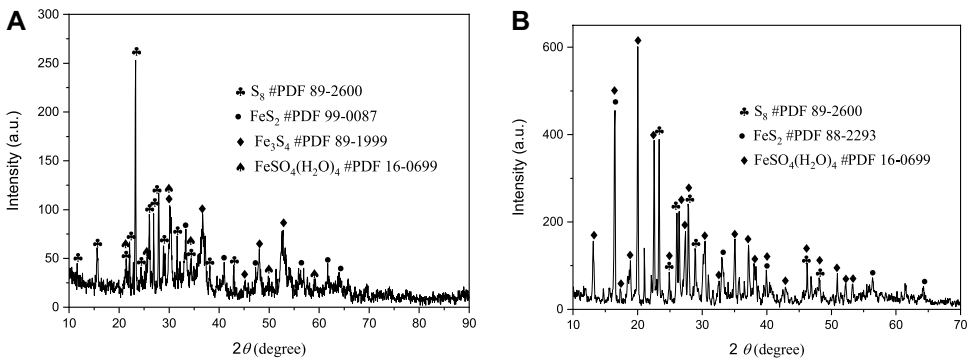

Fig. 3 Chemical composition of deposit in breathing pipe: **a** well TB101-X1; **b** well L14

breathing pipes of wells TB101-X1 and L14 because the precipitation kinetics are much faster for ferrous sulfide than for iron carbonate. Because of the low solubility of iron sulfide, which is several orders of magnitude lower than other common oilfield scales such as calcite ($CaCO_3$) or siderite ($FeCO_3$) (Pagenkop 1978; Lu et al. 2010; Hamid et al. 2016; Bryndzia et al. 2020), iron sulfide scale can easily form. Moreover, the solubility limit of ferrous sulfide is lower (Marcus et al. 1990; Zheng et al. 2016). Therefore, a ferrous sulfide thin film was formed initially on the surface of the steel, followed by damage and breakdown of the thin ferrous sulfide layer, which lead to pit initiation. The role of CO_2 in high content of hydrogen sulfide-containing natural gas is to supply the H^+ buffering effect supplied by H_2CO_3 to propagate the pit (Zhang et al. 2021).

Scale formation model

Elemental sulfur formation model

The dissolution and deposition of elemental sulfur in sulfide-containing natural gas are a pair of reversible processes (Eq. 1). When the temperature and pressure of the fluid increase, the reaction proceeds toward the formation of hydrogen polysulfide (H_2S_{x+1}), and the solubility of elemental sulfur in natural gas increases. Conversely, when the fluid temperature and pressure decrease, hydrogen polysulfide is decomposed into H_2S and elemental sulfur (Roberts 1997).

$$H_2S_{1+x} \rightleftharpoons H_2S_g + S_x. \tag{1}$$

When the reaction in Eq. 1 is in an equilibrium state, the reaction equilibrium constant can be expressed by Eq. 2,

$$K_{H_2S_{1+x}} = \frac{[H_2S_g][S_x]}{[H_2S_{1+x}]} \tag{2}$$

where $K_{H_2S_{1+x}}$ is the equilibrium constant of reaction (mol/L) in Eq. 1; $[S_x]$ is the elemental sulfur solubility in sulfide-containing natural gas (mol/L); $[H_2S_{1+x}]$ is the content of hydrogen polysulfide in the gas (mol/L); and $[H_2S_g]$ is the content of hydrogen sulfide in the gas (mol/L).

Based on previous studies (Chrastil 1982; Roberts 1997), the temperature dependence of the equilibrium constant $K_{H_2S_{1+x}}$ (Jiang et al. 2012) is expressed by Eq. 3:

$$-4.5711) \tag{3}$$

where T_K is the absolute temperature (K).

The conversion reaction between hydrogen sulfide in the gas and hydrogen sulfide in the produced water is given by Eq. 4:

$$H_2S_g. \tag{4}$$

Additionally, the equilibrium constant of the reaction is given by Eq. 5:

$$K_{H_2S} = \frac{[H_2S_{aq}]}{[H_2S_g]} \tag{5}$$

where $[H_2S_{aq}]$ is the concentration of hydrogen sulfide dissolved in the produced water (mol/L). The equilibrium constant K_{H_2S} is temperature-dependent (Suleimenov and Krupp 1994) and is given by,

$$K_{H_2S} = 10^{634.27+0.2709T_K-1.11132\times10^{-4}T_K^2-16719/T_K-261.9\log T_K}. \tag{6}$$

where T_K is expressed in Kelvin.

Combining Eqs. 2 and 5, Eq. 7 is obtained,

$$[S_x] = \frac{K_{H_2S_{1+x}}[H_2S_{1+x}]K_{H_2S}}{[H_2S_{aq}]}. \tag{7}$$

In the flow process of sulfide-containing gas, the elemental sulfur solubility in the gas, $[S_x]$, will decrease with decreasing temperature and pressure. Consequently, the undissolved elemental sulfur in the gas precipitates and gets deposited.

Ferrous polysulfide scale formation model

When hydrogen sulfide is dissolved in a thin liquid film, it decomposes according to Eq. 8,

$$H_2S_{aq} \rightleftharpoons H^+ + HS^-_{aq}. \tag{8}$$

The equilibrium constant $K_{a,1}$ (mol/L) is expressed as,

$$K_{a,1} = \frac{[H^+]\left[HS^-_{aq}\right]}{[H_2S_{aq}]} \tag{9}$$

where the temperature-dependent equilibrium constant $K_{a,1}$ is given by (Suleimenov and Steward. 1997) as:

$$K_{a,1} = 10^{\left[782.43945+0.361261T_K-1.6722\times10^{-4}T_K^2-\left(\frac{20565.7315}{T_K}\right)-(142.741722\ln T_K)\right]}. \tag{10}$$

With an increase in pH, more sulfide ions are produced. When iron corrodes in a thin liquid film resulting from the precipitation of the produced water carried by sulfide-containing natural gas, ferrous ions are generated. Once the concentration of ferrous ions exceeds the required concentration for scale formation, ferrous polysulfide precipitates in the thin liquid film according to Eqs. 11 and 12. Conversely, ferrous polysulfide also dissolves in a hydrogen-ion-containing environment,

$$Fe^{2+}_{aq} + H_2S_{aq} + S_0 \rightarrow FeS_2 + 2H^+_{aq}. \tag{11}$$

$$3Fe^{2+}_{aq} + 3HS^-_{aq} + S_0 \rightarrow Fe_3S_4 + 3H^+_{aq} \tag{12}$$

At constant temperature and pH, ferrous polysulfide is precipitated when the activity product of ferrous ions and sulfide ions, $\frac{\left[Fe^{2+}_{aq}\right][H_2S_{aq}]}{\left[H^+_{aq}\right]^2}$ and $\frac{\left[Fe^{2+}_{aq}\right]^3\left[HS^-_{aq}\right]^3}{\left[H^+_{aq}\right]^3}$, is higher than the solubility product constants of $K_{sp,\,FeS_2}\left(10^{-16.4}\right)$ and $K_{sp,\,Fe_3S_4}\left(10^{-12.84}\right)$ at 25℃ (Richard and Luther 2007), irrespectively.

Ferrous sulfate scale formation model

Ferrous ions produced during iron corrosion combine with sulfate ions to produce ferrous sulfate,

$$Fe^{2+} + SO_4^{2-} \rightarrow FeSO_4. \quad (13)$$

When the reaction is in equilibrium, the relationship between the solubility product constant and the product of the ion activity $[Fe^{2+}]_{eq}$ and $\left[SO_4^{2-}\right]_{eq}$ is given by Eq. 14:

$$K_{sp,FeSO_4} = \left[Fe^{2+}\right]\left[SO_4^{2-}\right] \quad (14)$$

However, the solubility product constant $K_{sp,FeSO_4}$ is temperature-dependent (Reardon et al. 1987) and is given by Eq. 15,

$$\log K_{sp,\,FeSO_4} = 1.447 - 0.004153T - \frac{214949}{T_K^2}. \quad (15)$$

When the activities of ferrous ions and sulfate ions in actual thin films satisfy the condition $\left[Fe^{2+}\right]\left[SO_4^{2-}\right] > K_{sp,\,FeSO_4}$, ferrous sulfate scale is precipitated.

Verification of deposit formation models

To verify the deposit formation models of elemental sulfur, ferrous polysulfide, and ferrous sulfate, the data of the chemical composition of precipitating water and sulfide-containing natural gas in the breathing pipe of the produced water tank of the TB101-X1 well were chosen as examples. The gas in the breathing pipe of the TB101-X1 well-produced water tanks was composed of methane (98.41%), ethane (0.24%), hydrogen sulfide (0.35%), and carbon dioxide (0.439%). The precipitating water exhibited a pH of 8.31, high degree of mineralization (52.66 g/ L), and primarily contained chloride, sodium, and sulfate ions (Table 1). The annual atmospheric temperature range of well TB101-X1 was large (−4.5–41.2 °C); additionally, the temperature variation of the breathing pipe was large. For example, the measured temperature of the breathing pipe in May 2020 was in the range 22.0–30.3 °C. Here, the activity coefficients were calculated by Pitzer theory (Lewis et al. 1961) for Fe^{2+}, H_2S_{1+x}, $H2S_{aq}$, $SO_4{}^{2-}$ and H^+ activity in calculating the activity product constant. PHREEQC or Visual Minteq did not consider in this paper because above software has big deviation of saturation index (SI) due to different activity coefficient model and lower K_{SP} (Liu 2017). The models in this paper are based on the Pitzer model; however, the other two software were based on SIT or Debye–Hückel expression or Debye–Hückel-modified expression.

Prediction of elemental sulfur formation

When $[H_2S_{1+x}]$ = 0.058 mmol/L and $[H_2S_{aq}]$ = 21.7 mmol/L, the change in solubility of elemental sulfur with temperature in sulfide-containing natural gas (Fig. 4) is established according to sulfur deposit model (Eq. 7). As shown in Fig. 4, the solubility of elemental sulfur increased linearly with the temperature of the gas. As the gas temperature of the breathing pipe decreased, the solubility of elemental sulfur decreased and supersaturated elemental sulfur was deposited from the gas. The higher the temperature drop in the gas flow process in the breathing pipe, the more the release of sulfur.

Prediction of ferrous polysulfide deposit formation

When $\left[Fe_{aq}^{2+}\right]$= 3.559 mmol/L, $\left[H_2S_{aq}\right]$=0.739 mg/L and pH = 8.31 during corrosion of iron, the change in $\frac{\left[Fe_{aq}^{2+}\right][H_2S_{aq}]}{[H_{aq}^{+}]^2}$ and $\frac{\left[Fe_{aq}^{2+}\right]^3\left[HS_{aq}^{-}\right]^3}{[H_{aq}^{+}]^3}$ with temperature can be obtained by using Eqs. 11 and 12 (Fig. 5). It can be seen from Fig. 5 that $\frac{\left[Fe_{aq}^{2+}\right][H_2S_{aq}]}{[H_{aq}^{+}]^2}$ and $\frac{\left[Fe_{aq}^{2+}\right]^3\left[HS_{aq}^{-}\right]^3}{[H_{aq}^{+}]^3}$ are larger than K_{sp,FeS_2} and K_{sp,Fe_3S_4} at 25℃, which indicates that the scaling occurs. And scaling probability of ferrous polysulfide increases with a decrease in temperature. However, the

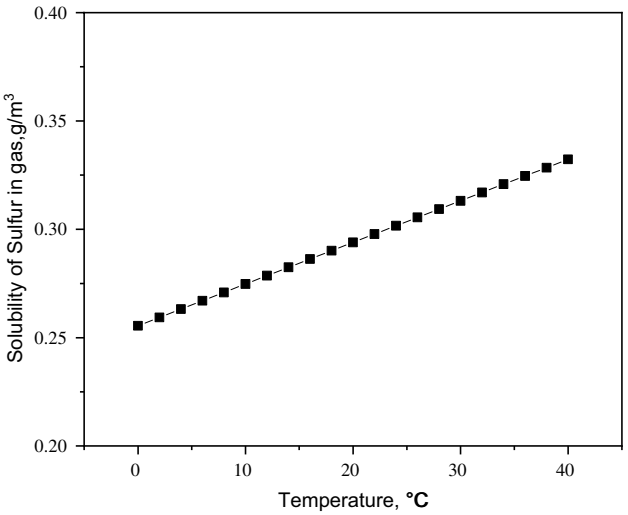

Fig. 4 Change in solubility of sulfur with temperature

Table 1 Chemical composition of the precipitating water in the breathing pipe of well TB101-X1 (mg/L)

Li^+	K^+	Na^+	Ca^{2+}	Mg^{2+}	Sr^{2+}	Fe^{2+}	Cl^-	Br^-	$SO_4{}^{2-}$	I^-	$HCO_3{}^-$	$CO_3{}^{2-}$	H_2S
8	245	18,723	650	40	14	1413	20,941	171	7781	34	3317	–	739

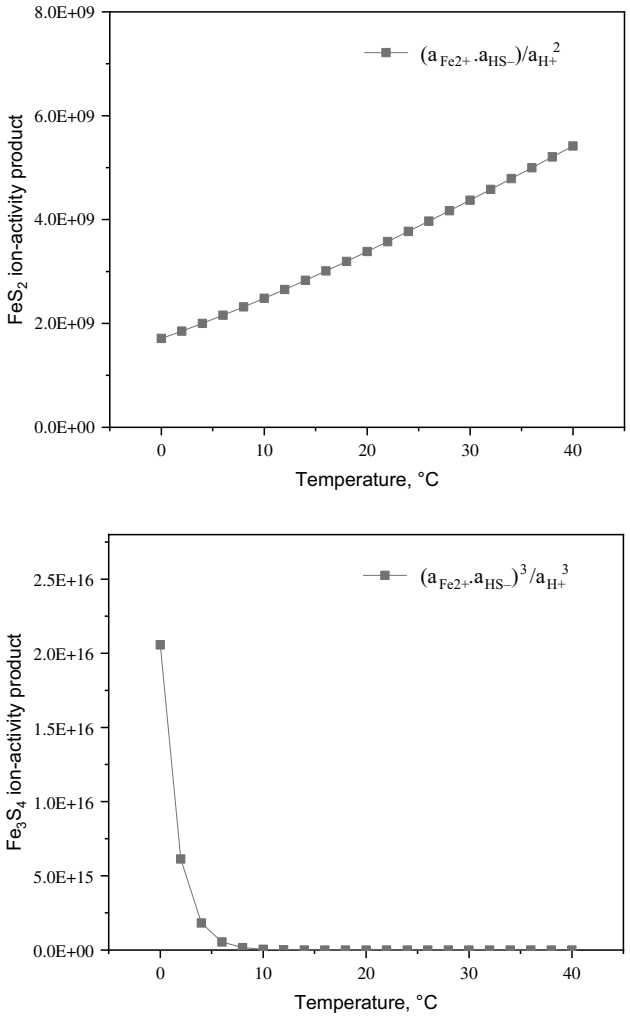

Fig. 5 Change in activity product and solubility product constants of ferrous polysulfide with temperature

scaling probability of the breathing pipe is obvious within the range of 0–40 °C.

Prediction of ferrous sulfate scale formation

Based on the ferrous sulfate formation model (Eq. 15), the evolution probability of ferrous sulfate at different temperatures (Fig. 6) was determined. As shown in Fig. 6, the solubility product constant of scale formation $K_{sp,FeSO_4}$ increased with increasing temperature. When the $[Fe^{2+}]$ activity in condensed water was lower than 34.82 mmol/L, ferrous sulfate had no scaling tendency in the precipitating water with 81.05 mmol/L $[SO_4^{2-}]$. In contrast, when the $[Fe^{2+}]$ ion concentration was higher than 34.82 mmol/L, ferrous sulfate had a scaling probability of 81.05 mmol/L $[SO_4^{2-}]$. Under the thin electrolyte film formed on the inner surface of pipe, iron ion continually produced in the process of hydrogen sulfide corrosion. The concentration of iron ion and sulfate increased in

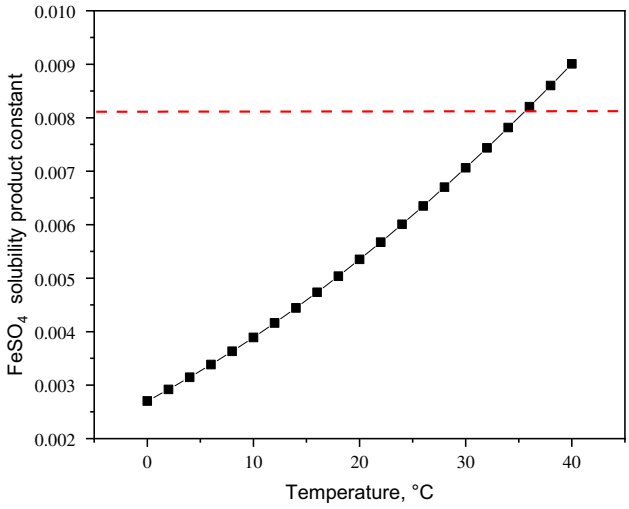

Fig. 6 Change in solubility product constant of ferrous sulfate with temperature

the film due to the evaporation of the water in the film with big change of temperature. For example, if the precipitating film contained 5600 mg/L $[Fe^{2+}]$ and 7781 mg/L $[SO_4^{2-}]$, then $[Fe^{2+}][SO_4^{2-}] = 0.0081$ (mol/L)^2 (shown as red dotted line in Fig. 6). This satisfies the condition $[Fe^{2+}][SO_4^{2-}] > K_{sp,FeSO_4}$ when the temperature is within the range of 0–35 °C; accordingly, ferrous sulfate was deposited. However, it did not satisfy the condition $[Fe^{2+}][SO_4^{2-}] > K_{sp,FeSO_4}$ within the range of 36–40 °C; accordingly, ferrous sulfate was not deposited.

According to the above deposit model prediction and validation (Fig. 3), the deposits in the breathing pipe of the produced water tank of the TB101-X1 well are composed of both the corrosion scale (ferric polysulfide and ferrous sulfate) and the elemental sulfur scale. The deposit formation prediction results are consistent with the actual composition of the deposit, which validates the accuracy and reliability of the deposit formation model.

Conclusion

1) The deposition of the breathing pipe in a sulfide-containing natural gas station is consisted of elemental sulfur and the corrosion scale of ferric polysulfide and ferrous sulfate.
2) The elemental sulfur scale in sulfide-containing natural gas is deposited with the decrease of the solubility of sulfur according to the thermodynamic deposit formation model of elemental sulfur.
3) The corrosion scales of ferrous polysulfide and ferrous sulfate form when the ion activity product exceeds the solubility product constant of ferrous polysulfide and ferrous sulfate according to the thermodynamic deposit

formation model of ferrous polysulfide and ferrous sulfate.

4) The larger amounts of elemental sulfur, ferrous polysulfide and ferrous sulfate are formed with larger temperature drop according to above thermodynamic deposit formation models.
5) The deposits of elemental sulfur, and the corrosion scale of ferrous polysulfide and ferrous sulfate were predicted to form in the breathing pipe of the produced water tank of the TB101-X1 well.

Funding The authors would like to acknowledge financial support from the Research Foundation of Northeast Sichuan Gas Field, PetroChina Southwest Oil and Gas Field (XNS-CDBQK-JS2020-014, JS2020-52).

Availability of data, Code and materials No dataset was generated or analyzed during this study.

Declarations

Conflict of Interests All authors disclosed no relevant relationships.

References

Ahmed ME, Hussein IA, Onawole AT et al (2020) Pyrite-scale removal using glutamic diacetic acid: a theoretical and experimental investigation. SPE Prod & Oper 36(3):751–759. https://doi.org/10.2118/204478-PA

Bryndzia LT, Villegas EI, Exploration SI (2020) Predicting the concentration of hydrogen sulfide in hydrocarbon-bearing clastic reservoirs: Introducing the iron-chlorite-pyrite-hydrogen sulfide model. SPE J 2020:3186–3199. https://doi.org/10.2118/201190-PA

Chrastil J (1982) Solubility of solids and liquids in supercritical gases. J Phys Chem C 86:3016–3021. https://doi.org/10.1021/j100212a041

Cifuentes L, Casas JM, Simpson J (2006) Temperature dependence of the speciation of copper and iron in acidic electrolytes. Chem Eng Res Des 84(10):965–969. https://doi.org/10.1205/cherd05047

Du Q (2016) Study of scaling mechanism and anti-scale models for natural gas gathering pipelines in northwest Sichuan gas field. Dissertation, Southwest Petroleum University.

Hamid S, De Jesús O, Jacinto C et al (2016) A practical method of predicting calcium carbonate scale formation in well completions. SPE Prod & Oper 31(1):1–11. https://doi.org/10.2118/168087-PA

Jiang X, Qu DR, Liu XH (2012) Study on deposition, corrosion and corrosion control of elemental sulfur in sour gas field. Corros Protec Petrochem Ind 29:5–8. https://doi.org/10.3969/j.issn.1007-015X.2012.04.003

Kan AT, Dai J, Deng G et al (2019) Recent advances in scale prediction: approach and limitations. SPE J. https://doi.org/10.2118/190754-PA

Lemire R, Berner U, Musikas C et al (2013) Chemical thermodynamics of iron, Part 1 Paris. Nuclear Energy Agency, France

Lewis GN, Randall M (1961) Thermodynamics. revised by K.S. Pitzer and L. Brewer. McGraw-Hill, New York

Liu JR, Song SF, Yang YS (2016) Scaling predicting of produced wastewater from daniudi gas field. Environ Protect Oil and Gas 26(5):14–17. https://doi.org/10.3969/j.issn.1673-3177.2008.04.018

Liu Y, Zhang Z, Bhandari N et al (2017) New Approach to study iron sulfide precipitation kinetics, solubility, and phase transformation. Ind Eng Chem Res 56(31):9016–9027. https://doi.org/10.1021/acs.iecr.7b01615

Liu Y (2017) Iron sulfide precipitation kinetics, solubility, phase transformation, and corrosion versus temperature and ionic strength." Diss., Rice University. https://hdl.handle.net/1911/96116

Lu H, Kan AT, Tomson MB (2010) Effects of monoethylene glycol on carbonate equilibrium and calcite solubility in gas/monoethylene glycol/NaCl/water mixed systems. SPE J. 15(3):714–725. https://doi.org/10.2118/121562-PA

Marcus P (1990) Potential-pH diagrams for adsorbed species. J Electrochem Soc 137:2709. https://doi.org/10.1149/1.2087025

Nasr-El-Din HA, Al-Humaidan AY (2001) Iron sulfide scale: formation, removal and prevention. paper presented at the International Symposium on Oilfield Scale, Aberdeen, UK, 30–31 January. SPE-68315-MS. https://doi.org/10.2118/68315-MS

Obot IB (2021) Under-deposit corrosion on steel pipeline surfaces: mechanism, mitigation and current challenges. J Bio Tribo Corros 7(14):40. https://doi.org/10.1007/s40735-021-00485-9

Pagenkop GK (1978) Introduction to natural water chemistry. New York City, New York, USA: M. Dekker

Ramanathan RS, Nasr-El-Din HA, Zakaria AS (2020) New insights into the dissolution of iron sulfide using chelating agents. SPE J. 25(06):3145–3159. https://doi.org/10.2118/202469-PA

Reardon E, Beckie R (1987) Modelling chemical equilibria of acid mine-drainage: The $FeSO_4$-H_2SO_4-H_2O system. Geochim Cosmochim Ac 51:2355–2368. https://doi.org/10.1016/0016-7037(87)90290-0

Rickard D, Luther GW (2007) Chemistry of iron sulfides. Chem Rev 107(2):514–562. https://doi.org/10.1021/cr0503658

Roberts BE (1997) The effect of sulfur deposition on gaswell inflow performance. SPE Reser Eng 12:118–123. https://doi.org/10.2118/36707-pa

Shahzad KM, Hussein I, Mahmoud M et al (2018) Oilfield scale formation and chemical removal: a review. J Petrol Sci Eng 171:127–139. https://doi.org/10.1016/j.petrol.2018.07.037

Shun H, Wang R, Lu Y (1999) Predicting technology and application methods on scale formation in oil and gas field. Fault Block Oil and Gas Fiels 6:40–43. https://doi.org/10.3969/j.issn.1005-8907.1999.04.019

Song SQ, Jiang SH, Zhang YZ et al (2011) Prevention of fouling in oil fields. Corros Protect Petrochem Ind 28:5–7. https://doi.org/10.3969/j.issn.1007-015X.2011.01.002

Suleimenov OM, Krupp RE (1994) Solubility of hydrogen sulfide in pure water and in NaCl solutions, from 20 to 320°C and at saturation pressures. Geochim Cosmochim Acta 58:2433–2444. https://doi.org/10.1016/0016-7037(94)90022-1

Suleimenov OM, Seward TM (1997) A spectrophotometric study of hydrogen sulphide ionisation in aqueous solutions to 350°C.

Geochim Cosmochim Acta 61:5187–5198. https://doi.org/10.1016/s0016-7037(97)00291-3

Tang QH, Tang L, Chen XP (2011) A review of scaling predicting models in oil and gas field. J Da Qing Norm Univers 31(06):60–63. https://doi.org/10.3969/j.issn.2095-0063.2011.06.017

Verri G, Sorbie KS, Singleton MA et al (2017) Iron sulfide scale management in high-H_2S and -CO_2 carbonate reservoirs. SPE Prod & Oper 32(3):305–313. https://doi.org/10.2118/179871-PA

Wang X, Dai Z, Ko S et al (2022) Iron sulfide solubility measurement and modeling over wide ranges of temperatures. Ionic Strength, and pH SPE J. https://doi.org/10.2118/208616-PA

Yu JQ, Jichao Z (1999) Using Oddo-Tomson's saturation index model to predict scaling in oil and gas well. Petro Geo Recov Efficien 6:79–86. https://doi.org/10.13673/j.cnki.cn37-1359/te.1999.01.016

Zhang W, Brown B, Young D et al (2021) Pitting mechanism of mild steel in marginally sour environments—Part I: a parametric study based on formation of protective layers. Corros Sci 183:109305. https://doi.org/10.1016/j.corsci.2021.109305

Zheng Y, Ning J, Brown B et al (2016) Advancement in predictive modeling of mild steel corrosion in CO_2 and H_2S containing environments. Corrosion 72:679–691. https://doi.org/10.5006/1667